Research article

NMR IN BIOMEDICINE

Received: 6 February 2015, Revised: 19 July 2015, Accepted: 27 July 2015, Published online in Wiley Online Library: 7 September 2015

(wileyonlinelibrary.com) DOI: 10.1002/nbm.3385

Histogram analysis of quantitative T_1 and MT maps from ultrahigh field MRI in clinically isolated syndrome and relapsing–remitting multiple sclerosis

Ali Al-Radaideh[a,b]*, Olivier E. Mougin[b], Su-Yin Lim[c], I-Jun Chou[c,d], Cris S. Constantinescu[c] and Penny Gowland[b]

This study used quantitative MRI to study normal appearing white matter (NAWM) in patients with clinically isolated syndromes suggestive of multiple sclerosis and relapsing–remitting multiple sclerosis (RRMS). This was done at ultrahigh field (7 T) for greater spatial resolution and sensitivity. 17 CIS patients, 11 RRMS patients, and 20 age-matched healthy controls were recruited. They were scanned using a 3D inversion recovery turbo field echo sequence to measure the longitudinal relaxation time (T_1). A 3D magnetization transfer prepared turbo field echo (MT-TFE) sequence was also acquired, first without a presaturation pulse and then with the MT presaturation pulse applied at −1.05 kHz and +1.05 kHz off resonance from water to produce two magnetization transfer ratio maps (MTR(−) and MTR(+)). Histogram analysis was performed on the signal from the voxels in the NAWM mask. The upper quartile cut-off of the T_1 histogram was significantly higher in RRMS patients than in controls ($p < 0.05$), but there was no difference in CIS. In contrast, MTR was significantly different between CIS or RRMS patients and controls ($p < 0.05$) for most histogram measures considered. The difference between MTR(+) and MTR(−) signals showed that NOE contributions dominated the changes found. There was a weak negative correlation ($r = -0.46$, $p < 0.05$) between the mode of T_1 distributions and healthy controls' age; this was not significant for MTR(+) ($r = -0.34$, $p > 0.05$) or MTR(−) ($r = 0.13$, $p > 0.05$). There was no significant correlation between the median of T_1, MTR(−), or MTR(+) and the age of healthy controls. Furthermore, no significant correlation was observed between EDSS or disease duration and T_1, MTR(−), or MTR(+) for either CIS or RRMS patients. In conclusion, MTR was found to be more sensitive to early changes in MS disease than T_1. Copyright © 2015 John Wiley & Sons, Ltd.

Keywords: ultrahigh field MRI; clinically isolated syndromes; relapsing–remitting multiple sclerosis; normal appearing white matter; nuclear Overhauser effect; relaxometry; quantitative magnetization transfer

INTRODUCTION

Changes in normal appearing white matter (NAWM) may be important in understanding the discrepancy observed between lesion load detected on MRI (1) and clinical status of multiple sclerosis (MS) patients. It is thought that this discrepancy is due to the diffuse, occult disease beyond the 'visible' white matter (WM) lesions, as well as grey matter (GM) disease (1,2).

Post mortem studies in MS have shown that NAWM is abnormal (3), and although the origin of these changes is unclear they are thought to be due to extensive glial pathology, microglial activation, axonal loss, and inflammatory cell infiltration. It has been argued that these changes either are due to primary events such as microglial activation-induced inflammation and axonal loss, or reflect degenerative events in NAWM due to axonal transection in lesions (secondary Wallerian degeneration) (4). Studies have shown that NAWM abnormalities increase with disease duration (5) and disability (6). Small focal abnormalities independent of the macroscopic lesions have also been seen in NAWM of MS patients (3).

Diffuse, occult disease cannot be detected using conventional MRI, as it is unable to detect microscopic changes, but diffuse pathology can be studied with quantitative MR (1) measures

* *Correspondence to: Ali Al-Radaideh, The Hashemite University, Medical Imaging, Zarqa, Jordan.*
E-mail: ali.radaideh@hu.edu.jo

a *A. Al-Radaideh*
Medical Imaging, The Hashemite University, Zarqa, Jordan

b *A. Al-Radaideh, O. E. Mougin, P. Gowland*
Sir Peter Mansfield Imaging Centre, University of Nottingham, Nottingham, UK

c *S.-Y. Lim, I.-J. Chou, C. S. Constantinescu*
Clinical Neuroscience, University of Nottingham, Nottingham, UK

d *I.-J. Chou*
Paediatric Neurology, Chang Gung Memorial Hospital, Taoyuan, Taiwan

Abbreviations used: *NAWM, normal appearing white matter; MTR, magnetization transfer ratio; NOE, nuclear Overhauser effect; CIS, clinically isolated syndrome; MS, multiple sclerosis; RRMS, relapsing–remitting MS; WM, white matter; GM, grey matter; DWI, diffusion weighted imaging; EDSS, Expanded Disability Status Scale; FS, Functional System; TFE, turbo field echo; MPRAGE, magnetization prepared rapid acquisition gradient echo; FLAIR, fluid attenuated inversion recovery; ASYM, asymmetry; FDR, false discovery rate; FWHM, full width at half maximum; APT, amide proton transfer; NABT, normal appearing brain tissue.*

including relaxometry, magnetization transfer ratio (MTR) and susceptibility mapping, diffusion weighted imaging (DWI), or MRS. It has been shown that most pathological changes occur in early relapsing–remitting MS (RRMS), and these changes can then play an important role in the degree of severity of MS disease. Techniques that could detect such early changes or even earlier changes in clinically isolated syndromes (CISs) (often indicative of MS) could assist in treating the disease prior to permanent disability.

The aim of this work is to study the changes in NAWM in patients at presentation with CISs suggestive of MS and RRMS patients compared with healthy controls, comparing T_1 and MTR MR measures. Data were acquired at high field (7 T) to give increased sensitivity and increased spatial resolution, which is needed to study heterogeneity in the WM. Two different MTR measures were acquired, one sensitive to standard MT effects from macromolecules (MTR(+)) and the second also sensitive to nuclear Overhauser effects (NOEs), probably arising from aliphatic protons in lipids associated with myelin (MTR(−)) (7,8).

MATERIALS AND METHODS

Subjects

17 patients with CIS (10 females, 7 males; mean age 37.9 years; age range 26–41), and 11 patients with RRMS (7 females, 4 males; mean age 42.6 years; age range 20–54 years) were recruited from Nottingham University Hospital, along with 22 age matched healthy controls (9 females, 13 males; mean age 36.6 years; age range 21–48). Of the 22 controls, only three subjects were staff from the MRI centre (two of whom were extremely familiar with the 7 T), one was a medical doctor who was naive to the 7 T, and the rest were friends of the patient group, who were probably less familiar with being scanned than the MS patients.

All participants gave informed consent according to local ethics approval. Table 1 summarizes the characteristics of the three groups. Of the CIS group, six presented with optic neuritis, three with myelitis, two with a brainstem syndrome, and six with a cerebral hemisphere presentation. All of the patients were treatment naive, and none had received corticosteroid treatment within the past 3 months. The neurological examination was done by a doctor qualified to perform EDSS (Expanded Disability Status Scale) assessments. A Functional System (FS) grade was obtained for each area representing a different function of the central nervous system (pyramidal, brain stem, visual, cerebellar, sensory, bowel and bladder, and higher cerebral). The FS scores reflected the degree of disability across all these areas, as found on the neurological assessment. The final EDSS score was calculated on the basis of the combined/summarized FS scores, giving a value of between 0 (normal examination) and 10 (death due to MS).

Table 1. Characteristics of study controls and subjects with CIS and RRMS

Subjects	Controls	CIS patients	RRMS patients
N	22	17	11
Sex, F/M	9/13	10/7	7/4
Mean age ± SD, years	36.55 ± 8.06	37.94 ± 9.3	42.6 ± 12.87
Age range, years	21–48	26–41	20–54
Mean EDSS ± SD	–	1.91 ± 1.08	3.26 ± 1.27
EDSS range	–	0–4	2–6.5
Mean disease duration ± SD, years	–	1.45 ± 1.18	13.16 ± 9.73
Disease duration range, years	–	0.4–4.5	1.67–34

Data acquisition

Scanning was performed on a 7 T Philips Achieva MR system, equipped with a 16-channel receive coil and head-only, volume transmit coil. MT weighted images were acquired using a 3D MT prepared turbo field echo (MT-TFE) sequence with $0.86 \times 0.86 \times 1.5$ mm voxel size; $T_E = 5.7$ ms; $T_R = 9.8$ ms; 20 slices (9). Three acquisitions were made: one with no presaturation, one with presaturation −1.05 kHz off resonance from water (sensitive to MT and NOEs, MTR(−)), and one with presaturation +1.05 kHz off resonance to give sensitivity primarily to MT (MTR(+)) (total scan time = 8 min 22 s for the three acquisitions). The pulsed saturation was applied as a train of off-resonance pulses applied at ±1.05 kHz (3.5 ppm). Each pulse train consisted of 20 Gaussian windowed 13.5 μT, sinc, 20 ms pulses with a bandwidth of 300 Hz and 55 ms between each pulse. T_1 maps were created from 3D inversion recovery TFE (IR-TFE) images (also known as MPRAGE images) (10) acquired at seven different inversion times (150, 300, 500, 800, 1200, 1800, 2500 ms). The acquisition parameters were the following: $T_E = 3.2$ ms; $T_R = 6.9$ ms; flip angle of the TFE readout pulse = 8°; TFE factor per inversion = 240; shot-to-shot interval = 8 s; spatial resolution = $1.25 \times 1.25 \times 1.25$ mm^3; field of view = $200 \times 200 \times 72.5$ mm^3; scan time per T_I = 2 min. An adiabatic, phase modulated inversion pulse with a bandwidth of 1.6 kHz and duration of 13 ms was used (11). A B_1 map was acquired using the two T_R method (12) to correct the MT images for the effect of B_1 inhomogeneity and to calculate the readout flip angles for T_1 mapping. No T_2 fluid attenuated inversion recovery (T_2-FLAIR) was acquired at 7 T at the time of data acquisition due to some technical issues. However, for 14 CIS and 5 RRMS patients, 3D T_2-FLAIR scans were acquired on a 3 T Philips Achieva MR system with the following imaging parameters: $1 \times 1 \times 3$ mm^3 voxel size; $T_E = 125$ ms; $T_R = 11\,000$ ms; turbo factor = 27; 50 slices; scan time = 5 min 52 s. These were used to verify the semi-automated segmentation of lesions adopted in this work.

Data analysis and post-processing

T_1 maps were calculated from the IR-TFE images as described previously (11). The MT images acquired at positive and negative frequency offset were co-registered to the reference scan acquired with no saturation pulse using rigid body registration with six degrees of freedom in FSL (FMRIB, Oxford, UK). MTR maps were then calculated on a voxel by voxel basis using

$$\mathrm{MTR}_{(-)} = \frac{(S_0 - S_{\mathrm{MT}(-)})}{S_0} \quad [1]$$

$$\mathrm{MTR}_{(+)} = \frac{(S_0 - S_{\mathrm{MT}(+)})}{S_0}. \quad [2]$$

The IR-TFE image that was acquired near the null point of GM was used to segment the GM and WM in SPM (http://www.fil.ion.ucl.ac.uk/spm/). This algorithm automatically segmented MS lesions as GM tissues. The segmented WM was displayed as a probability map, which was converted to a mask and then eroded by two voxels to exclude any partial volume effects at the GM or lesion borders. Hereafter this mask will be referred to as a NAWM mask.

The reference volume in the MT sequence was then co-registered to the IR-TFE image used to create the NAWM mask, with rigid-body image registration using the FLIRT linear registration algorithm from the FSL platform (FMRIB). Because of the difference in contrast between the IR-TFE image and reference scan, the cost function was the "mutual information" with a low number (100) of bins. The registration matrix was applied to the registered MTR(−) and MTR(+) maps to transfer them into the same space as the IR-TFE image. Finally, the NAWM mask was then used to extract the NAWM tissue values from the T_1, MTR (−), and MTR(+) maps.

Both MTR(−) and MTR(+) were found to depend strongly on B_1 amplitude, such that the peripheral WM tended to have lower MTR values than the more central parts regardless of any abnormalities. Therefore, the relative effect of B_1 field inhomogeneity on MTR values within the NAWM mask was corrected using a method described by Ropele *et al.* (13).

Maps indicating the asymmetry of the MT spectrum (asymmetry maps, which will be dominated by NOE effects) were calculated on a voxel by voxel basis for the NAWM using the following equation:

$$\begin{aligned} \mathrm{ASYM}_{\mathrm{NAWM}} = {} & \text{corrected } \mathrm{MTR}(-)_{\mathrm{NAWM}} \\ & - \text{corrected } \mathrm{MTR}(+)_{\mathrm{NAWM}}. \end{aligned} \quad [3]$$

The asymmetry of the *z*-spectrum can theoretically measure NOE effects, but in practice it is confounded by a number of factors and is potentially noisy due to B_0 inhomogeneity. Nonetheless, it provides a convenient method to investigate other contributions to the *z*-spectrum. Color coded maps were produced in MATLAB to show the spatial distribution of T_1, MTR(−), MTR(+), and $\mathrm{ASYM}_{\mathrm{NAWM}}$ values within the NAWM masks. The lower and upper limits of the T_1, MTR and ASYM histograms were [500, −2000 ms], [0.1, −0.7], and [0, −0.2], respectively, and the histograms were normalized by the size of the NAWM mask.

To parameterize the shape of each histogram for each subject, the median, full width at half maximum (FWHM), and peak position (mode) were calculated, and the T_1 or MTR value corresponding to the cut-off for the upper quartile of the T_1 histogram and lower quartile of the MTR histograms was calculated. The median and peak positions of the histograms were plotted against age for healthy controls, and against EDSS and disease duration for CIS and RRMS patients separately. An averaged histogram was produced for each MRI measurement, for each group of subjects.

Joint histograms (scatter plots) of MTR(−) versus T_1 values within the NAWM masks were plotted against each other on a voxel by voxel basis for all slices for each subject to investigate any correlation between these parameters. Similar joint histograms were created for MTR(−) and MTR(+).

All statistical analysis was performed in SPSS 17.0 (SPSS, Chicago, IL, USA). Normality was tested using the Kolmogorov–Smirnov test. One way ANOVA with Tukey post hoc test was performed on the parametric data and the Kruskal–Wallis with Mann–Whitney pairwise multiple comparisons test was performed on non-parametric data. The significance level in the multiple comparisons between groups was calculated using a false discovery rate (FDR) test. Correlation coefficients were calculated using Pearson correlation.

The reproducibility of T_1 maps was tested by scanning the same healthy subject on five occasions. Another healthy subject was scanned five times with the MT-TFE and B_1 mapping sequences. Masking and histogram analysis was applied to each repeated data set as above.

RESULTS

Figure 1 shows T_1, MTR(−), MTR(+), and ASYM maps of the NAWM for the same three age matched subjects (control, CIS, and RRMS). Blue color was assigned to long T_1 and low MTR and ASYM values, since these are thought to correspond to abnormal changes in NAWM in MS. These maps are from three typical subjects, but similar trends in T_1, MTR, and ASYM between patient groups were found in all subjects, as indicated by the subject averaged histograms of the NAWM values shown

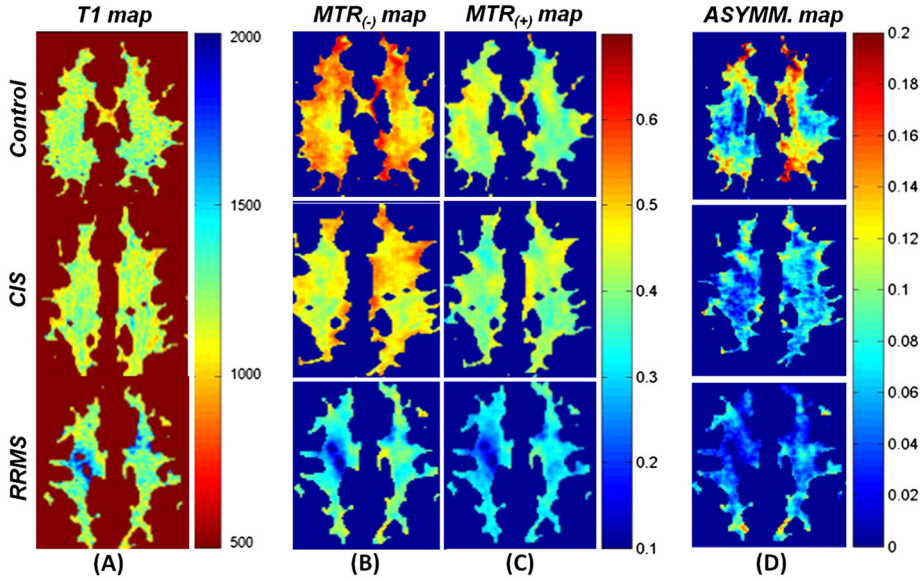

Figure 1. Representative T_1 (A), MTR(−) (B), MTR(+) (C), and asymmetry (D) maps of the NAWM for three age matched subjects (control, CIS, and RRMS).

NMR IN BIOMEDICINE

in Figure 2. The T_1 maps from the control and CIS patient are very similar, whereas the RRMS patient shows both diffuse and perilesional increase in T_1 values. In contrast, the differences in MTR between groups are more obvious, although this is particularly clear in the RRMS patient around the lesions. Similar trends are seen for MTR(+) and MTR(−), although the MTR(+) values are generally lower than those for MTR(−). Figures 1(d) and 2(c) demonstrate that the RRMS and CIS patients show less MTR asymmetry than do the control subjects.

Figure 3 plots the values of the median, peak position, and FWHM and the position of the upper/lower quartile of the T_1/MTR NAWM histograms for each subject in the three groups. The mean value of each parameter for each group is indicated by the red dash. Table 2 summarizes the statistical comparison of these measures between the three groups. For the T_1 histograms, only the upper quartile measure showed a significant difference ($p < 0.05$) between groups, being significantly larger in RRMS than in CIS patients or controls with a weak trend toward being larger in CIS patients than controls. This change in the tail of the histograms was consistent with the local changes seen around lesions in the maps in Figure 1. For the MTR(−) histograms, all measures except FWHM were significantly different between

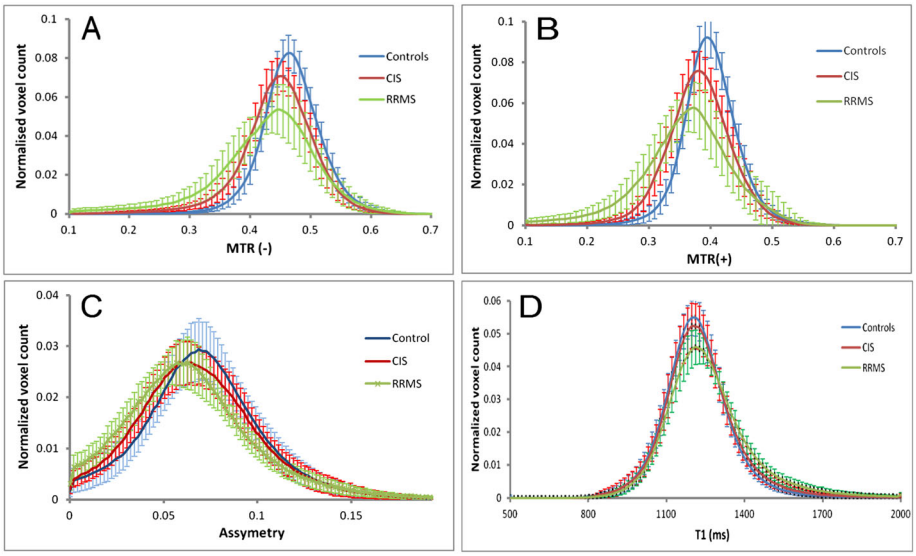

Figure 2. Normalized MTR(−) (A), MTR(+) (B), asymmetry (C), and T_1 (D) averaged histograms of the NAWM for the three groups of subjects.

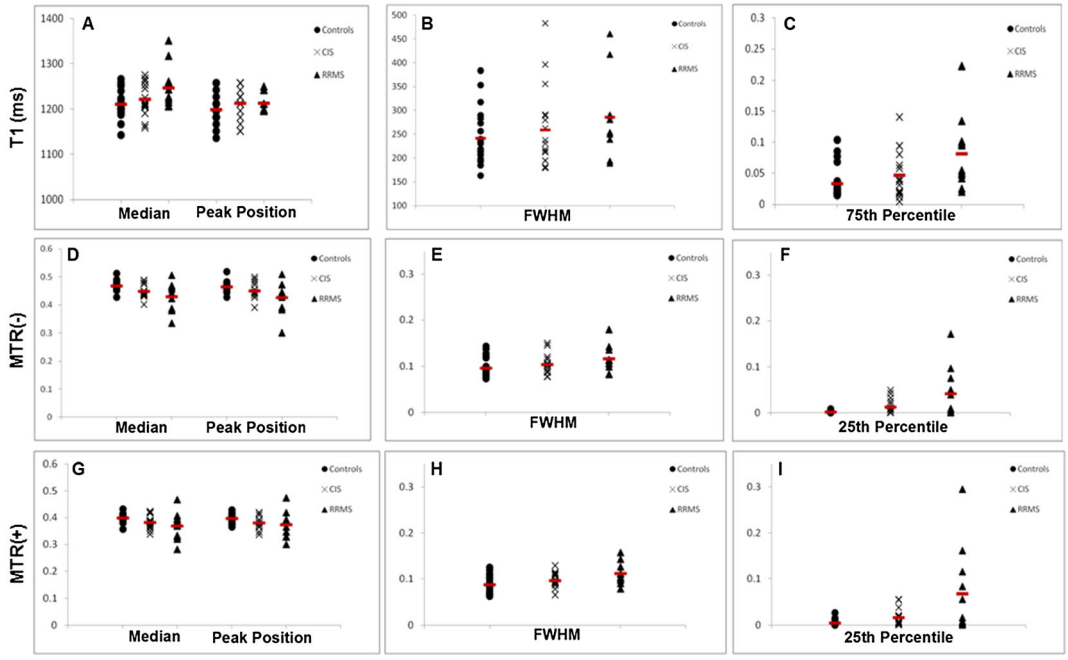

Figure 3. The median, peak position (A, D, and G), FWHM (B, E, and H), '75th percentile' (C), and '25th percentile' (F and I) statistics derived from each subject's T_1, MTR(−), and MTR(+) histograms for each of the three groups.

Table 2. Comparison of variation in parameters describing histograms between study groups

Value	Statistics	Between groups	*P* value corrected for multiple comparisons		
			Controls –CIS	Controls –RRMS	CIS –RRMS
T_1	Median	*>0.05*			
	Peak position	*>0.05*			
	FWHM	*>0.05*			
	Upper quartile cut-off	<0.05	*0.300*	0.003	0.036
MTR(−)	Median	<0.05	0.004	0.021	*0.578*
	Peak position	<0.05	0.017	0.024	*0.329*
	FWHM	*>0.05*			
	Lower quartile cut-off	<0.05	0.001	0.001	*0.306*
MTR(+)	Median	<0.05	0.003	0.017	*0.661*
	Peak position	<0.05	0.008	*0.053*	*0.746*
	FWHM	<0.05	*0.320*	0.002	*0.104*
	Lower quartile cut-off	<0.05	0.005	0.002	*0.225*

groups. However, the pairwise comparisons showed that these measures were significantly different between controls and CIS or RRMS patients but not between the CIS and RRMS patients. For the MTR(+) histograms, all measures were significantly different between groups. The pairwise comparisons showed that both the median and lower quartile were significantly different between controls and CIS or RRMS patients. The peak position was significantly different between controls and CIS patients, with a trend towards a difference between the controls and RRMS patients, whilst the FWHM only showed a significant difference between controls and RRMS. Again, no significant difference was found in any measure between CIS and RRMS patients.

Figure 4 shows that there was a weak negative correlation ($r = -0.46$, $p < 0.05$) between the peak position of the T_1 histogram and the age of healthy controls, but this was not significant for MTR(+) ($r = -0.34$, $p > 0.05$) or MTR(−) ($r = 0.13$, $p > 0.05$). There was no significant correlation between the median of T_1, MTR(−), or MTR(+) and the age of healthy controls. Furthermore, no significant correlation was observed between EDSS or disease duration and T_1, MTR(−), or MTR(+) for either CIS or RRMS patients.

Figure 5 shows the joint histogram of T_1 and MTR(−) for the three subjects illustrated in Figure 1. Again this shows that CIS resulted in reduced MTR(−) but not increased T_1, and RRMS showed a larger reduction in MTR(−) combined with a smaller increase in T_1 but with some NAWM voxels showing significant changes in both parameters. Similar trends were found in joint histograms for the other subjects.

Figure 6 shows a similar joint histogram of MTR(+) versus MTR(−) and demonstrates that these two measures are correlated, particularly for the RRMS patients. Since MTR(−) is sensitive to both MT and NOE effects, it will tend to be larger than MTR(+) in healthy NAWM. Therefore, the slope of this plot is expected to be less than unity averaging over all subjects. The average gradients of these scatter plots for the control, CIS, and RRMS subjects were 0.849 ± 0.021, 0.85 ± 0.026, and 0.86 ± 0.022, respectively (assuming zero intercept).

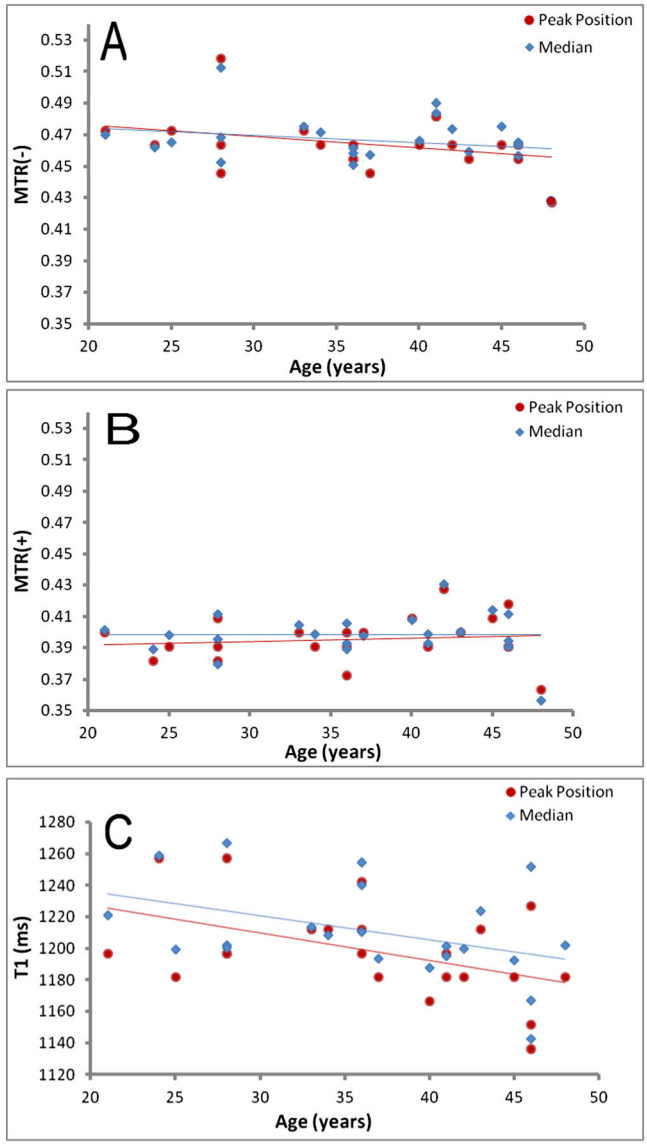

Figure 4. Correlation between the age and both peak position and median of MTR(−) (A), MTR(+) (B), and T_1 (C) histograms derived from the NAWM of healthy controls.

Table 3 summarizes the results of five repeated measurements of the T_1 histograms of the NAWM of one healthy control and the MTR histograms of the NAWM of another healthy control.

DISCUSSION

This work has shown that MT MR measures are sensitive to changes in NAWM in an earlier stage of demyelinating disease than are T_1 measures.

The study was carried out at ultrahigh field (7 T) to give increased sensitivity to MTR changes in particular, and also to allow data to be acquired with smaller voxels, providing better information about the heterogeneity of any changes occurring in WM. However, it is likely that these results can be used to optimize 3 T acquisitions to allow these methods to be translated to 3 T.

This is the first study in which MTR was measured in MS with saturation at two different frequencies placed symmetrically

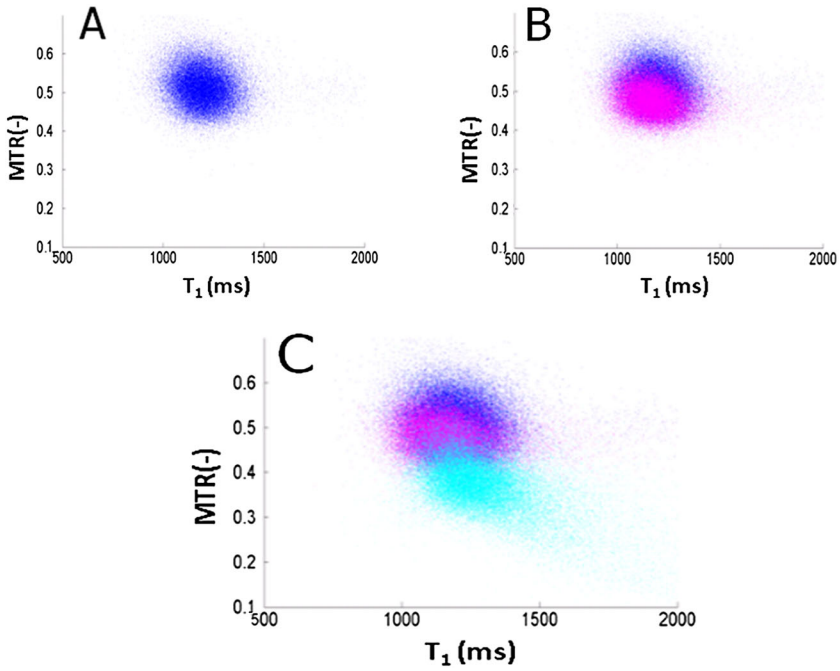

Figure 5. Joint histogram of MTR(−) versus T_1 for the control (blue), CIS (magenta), and RRMS (cyan) subjects shown in Figure 1. The histograms are overlaid, but also shown separately as insets for clarity.

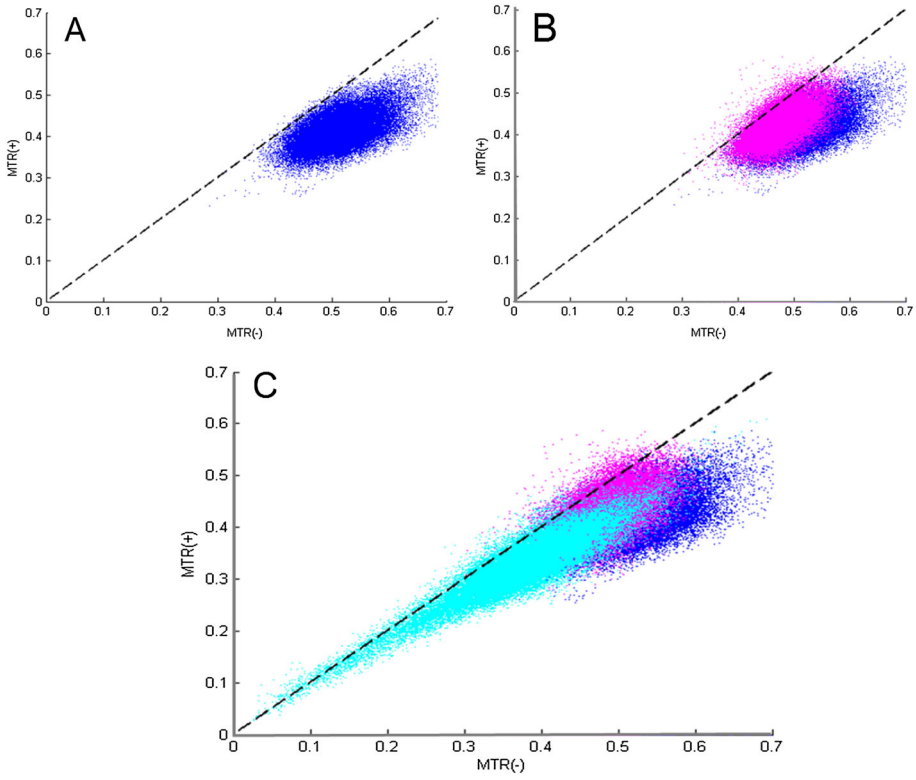

Figure 6. Joint histogram of MTR(−) versus MTR(+) for the control (blue), CIS (magenta), and RRMS (cyan) subjects shown in Figure 1. The histograms are overlaid, but also shown separately as insets for clarity.

about the water resonance. The positive frequency offset saturation (MTR(+)) produces images that are largely sensitive to MT with the semisolid proton pool related to macromolecules. It also has some sensitivity to chemical exchange saturation transfer effects, particularly from amide proton transfer (APT) at this frequency offset and power, although the APT signal is generally associated with increased protein synthesis and therefore is not expected to be particularly large in either healthy brain tissue or MS. However saturation at the negative offset (MTR(−)) produces images that also have some sensitivity to the NOE, which is

Table 3. Coefficient of variance (%) of the repeated measures of T_1, MTR(−), and MTR(+)

Statistics	T_1	MTR(−)	MTR(+)
Median	0.3	2.9	4.4
Peak position	0.1	3.7	3.4
FWHM	0.8	3.7	13.6

thought to be due to aliphatic protons, probably associated with lipids, and since distribution of the NOE signal in the brain is similar to the distribution of WM it is assumed that NOE is related to myelination (7). It should be noted that in both cases, for the sequence used here, MT with the semisolid proton pool will dominate over APT or NOE effects. MTR(−) was generally greater than MTR(+) in all groups, implying that the combined effects of NOE and MT were larger than the effects of APT and MT, as expected in the normal brain (8), so the asymmetry image (ASYM) is largely sensitive to NOE. The proper way to investigate different contributions to the MTR signals would be to acquire a *z*-spectrum showing the effect of off-resonance saturation at a range of frequencies and RF pulse amplitudes, but this would be very time consuming and would not currently be feasible at such high spatial resolution.

Significant differences between the three groups of subjects were found in histograms of NAWM from all these maps, with MT changes apparent earlier in disease progression (in CIS patients rather than in RRMS patients), as shown by the color maps (Fig. 1), the subject averaged histograms (Fig. 2), the summary measures from the histograms (Table 2 and Fig. 3) and the joint histograms between T_1 and MTR(+) (Fig. 5). Analysis of the ASYM maps (not shown) found no statistically significant difference in ASYM between the three groups, except that the ASYM peak position was significantly lower in RRMS than in CIS subjects, and a similar trend is seen in Figure 6 (suggesting smaller NOE contribution in RRMS). This variability apparent in the asymmetry map shown in Figure 1 was characteristic of the data from other subjects and is probably due to the noisiness of this measure and the effect of B_1 and B_0 inhomogeneities. Further work using full fitting of the *z*-spectrum will better characterize the NOE.

A weak negative correlation between peak position of T_1 measures and age was found for healthy subjects. Similar changes have been observed for T_1 across this age range (14). This is likely to be related to known iron accumulation during childhood, which continues into middle age (15). It is interesting that no such age related change was seen in MTR(+) or MTR(−), suggesting that there was no significant change in myelination over this age range, which is expected, although this experiment will be underpowered to detect a small change. No significant correlation was detected between the EDSS or disease duration and averaged T_1, MTR(−), or MTR(+) values, which could be due to the heterogeneity of the disease, the small sample size, the limited range of EDSS and disease durations, or the limited brain region studied here.

It was not feasible to acquire reproducibility data on patients, first as it would be too much burden on them and second because we cannot be sure that their brain signals are stable. Therefore, reproducibility was assessed in two healthy controls (one for T_1 and the other for MTR mapping), and the results showed that the repeatability of histogram measures was better for T_1 than MTR(−) or MTR(+). This is probably due to the noisiness of the MTR data and its sensitivity to B_1 and B_0, although it is notable that the MTR maps appeared to show more spatial variation than the T_1 maps. Some of these sources of variation could be overcome by full fitting to the *z*-spectrum if this could be achieved in a clinically appropriate scan time. A further possible cause of variation is the definition of the NAWM mask, which was created separately for each repeat. To test this, for 17 healthy and 14 CIS subjects, the NAWM was further eroded by an extra two voxels and the histograms were re-plotted, but this led to no significant change in the results.

These data were segmented on the 7 T MPRAGE, but it is possible that the MPRAGE scans underestimated the size of the lesions compared with a conventional FLAIR scan. For 14 CIS and 5 RRMS patients, on whom 3 T FLAIR scans were also acquired, a trained neurologist manually segmented the boundary of the lesions in the FLAIR images and the analysis was repeated on a new mask based on these boundaries. The results showed no significant difference between the two approaches to lesion segmentation. There was a reduced trend for a change in T_1 values, indicating that T_1 changes occur more perilesionally than MTR changes, which tend to affect larger regions of WM (as indicated in Figure 1).

RELATION TO OTHER WORK

Abnormalities in T_1 and T_2 relaxation times (5,16–22), MT (6,19,23–27), diffusion weighting (28), and spectroscopy have previously been reported in NAWM of MS patients, with some studies showing that these NAWM abnormalities increase with disease duration (5) and disability (6). The increase in T_1 values in NAWM in MS has been related to the effects of demyelination, gliosis, axonal loss, and edema on the mobile water pool (29–33). However, macrophage activity and metal deposition will decrease T_1, possibly limiting the sensitivity of T_1 mapping for detecting changes in MS (34,35), and its specificity to demyelination (36).

Some studies have failed to detect changes in MTR, reflecting how sensitive this parameter is to the exact pulse sequence used (18,37,38). However most studies have indicated that MTR is decreased in both MS lesions and normal appearing brain tissue (NABT) (39). This has been attributed to processes such as demyelination, axonal loss, and swelling, which lead to a decrease in the concentration of macromolecules.

Fewer studies have been performed in CIS patients. Several studies have reported reductions in MTR of NAWM (40,41) or NABT (25,42) in CIS patients compared with controls. However, others (43,44) found no change in MTR in the NAWM of CIS patients even within carefully selected ROIs. Changes in myo-inositol have also been detected in early CIS (45), but this has not been found by another group, maybe due to a smaller sample size (46,47). There are again mixed results with diffusion based measures, with some studies finding changes (48–50) and others not (51,52), sometimes even for the same measures. Another study has shown no change in T_2' (possibly related to oxygenation) in CIS (53), but another has noted a reduction in NAWM perfusion (54). To the best of our knowledge, this is the first study that investigates the T_1 relaxation time along with MTR at both offsets in NAWM of the CIS patient for ultra-high field MRI.

This group of subjects will be followed up over three years to determine whether NAWM changes locally or globally are

predictive of disease progression, as has been previously found for MTR changes in CIS patients (25).

Acknowledgements

This work was funded by the Medical Research Council and Engineering and Physical Sciences Research Council, UK. The 7 T scanner was funded by the Welcome Trust and the Higher Education Funding Council.

REFERENCES

1. Kappos L, Moeri D, Radue EW, Schoetzau A, Schweikert K, Barkhof F, Miller D, Guttmann CRG, Weiner HL, Gasperini C, Filippi M, for the Gadolinium MRI Meta-analysis Group. Predictive value of gadolinium-enhanced magnetic resonance imaging for relapse rate and changes in disability or impairment in multiple sclerosis: a meta-analysis. Lancet 1999; 353: 964–969.
2. Molyneux PD, Barker GJ, Barkhof F, Beckmann K, Dahlke F, Filippi M, Ghazi M, Hahn D, MacManus D, Polman C, Pozzilli C, Kappos L, Thompson AJ, Wagner K, Yousry T, Miller DH. Clinical–MRI correlations in a European trial of interferon beta-1b in secondary progressive MS. Neurology 2001; 57: 2191–2197.
3. Filippi M, Tortorella C, Bozzali M. Normal-appearing white matter changes in multiple sclerosis: the contribution of magnetic resonance techniques. Mult. Scler. 1999; 5: 273–282.
4. Miller DH, Thompson AJ, Filippi M. Magnetic resonance studies of abnormalities in the normal appearing white matter and grey matter in multiple sclerosis. J. Neurol. 2003; 250: 1407–1419.
5. Lacomis D, Osbakken M, Gross G. Spin–lattice relaxation (T_1) times of cerebral white matter in multiple sclerosis. Magn. Reson. Med. 1986; 3: 194–202.
6. Filippi M, Campi A, Dousset V, Baratti C, Martinelli V, Canal N, Scotti G, Comi G. A magnetization transfer imaging study of normal-appearing white matter in multiple sclerosis. Neurology 1995; 45: 478–482.
7. Wilhelma MJ, Onga HH, Wehrlib SL, Cheng L, Tsaia P-H, Hackneyc DB, Wehrlia FW. Direct magnetic resonance detection of myelin and prospects for quantitative imaging of myelin density. Proc. Natl. Acad. Sci. U. S. A. 2012; 109: 9605–9610.
8. Mougin O, Clemence M, Peters A, Pitiot A, Gowland P. High-resolution imaging of magnetisation transfer and nuclear Overhauser effect in the human visual cortex at 7 T. NMR Biomed. 2013; 26: 1508–1517.
9. Mougin OE, Coxon RC, Pitiot A, Gowland PA. Magnetization transfer phenomenon in the human brain at 7 T. Neuroimage 2010; 49: 272–281.
10. Deichmann R, Josephs O, Ashburner J, Turner R, Good CD. Optimization of 3-D MP-RAGE sequences for structural brain imaging. Neuroimage 2000; 12: 112–127.
11. Wright PJ, Mougin OE, Totman JJ, Peters AM, Brookes MJ, Coxon R, Morris PE, Clemence M, Francis ST, Bowtell RW, Gowland PA. Water proton T_1 measurements in brain tissue at 7, 3, and 1.5 T using IR-EPI, IR-TSE, and MPRAGE: results and optimization. Magn. Reson. Mater. Phys. Biol. Med. 2008; 21: 121–130.
12. Yarnykh VL. Actual flip-angle imaging in the pulsed steady state: a method for rapid three-dimensional mapping of the transmitted radiofrequency field. Magn. Reson. Med. 2007; 57: 192–200.
13. Ropele S, Filippi M, Valsasina P, Korteweg T, Barkhof F, Tofts PS, Samson R, Miller DH, Fazekas F. Assessment and correction of B_1-induced errors in magnetization transfer ratio measurements. Magn. Reson. Med. 2005; 53: 134–140.
14. Cho S, Jones D, Reddick WE, Ogg RJ, Steen RG. Establishing norms for age-related changes in proton T_1 of human brain tissue in vivo. Magn. Reson. Imaging 1997; 15: 1133–1143.
15. Hallgren B, Sourander P. The effect of age on the non-haemin iron in the human brain. J. Neurochem. 1958; 3: 41–51.
16. Barbosa S, Blumhardt LD, Roberts N, Lock T, Edwards RH. Magnetic resonance relaxation time mapping in multiple sclerosis: normal appearing white matter and the "invisible" lesion load. Magn. Reson. Imaging 1994; 12: 33–42.
17. Vaithianathar L, Tench CR, Morgan PS, Lin X, Blumhardt LD. White matter T_1 relaxation time histograms and cerebral atrophy in multiple sclerosis. J. Neurol. Sci. 2002; 197: 45–50.
18. Vrenken H, Geurts JJG, Knol DL, van Dijk LN, Dattola V, Jasperse B, van Schijndel RA, Polman CH, Castelijns JA, Barkhof F, Pouwels PJW. Whole-brain T1 mapping in multiple sclerosis: global changes of normal-appearing gray and white matter. Radiology 2006; 240: 811–820.
19. Vrenken H, Geurts JJG, Knol DL, Polman CH, Castelijns JA, Pouwels PJW, Barkhof F. Normal-appearing white matter changes vary with distance to lesions in multiple sclerosis. Am. J. Neuroradiol. 2006; 27: 2005–2011.
20. Vrenken H, Rombouts SARB, Pouwels PJW, Barkhof F. Voxel-based analysis of quantitative T1 maps demonstrates that multiple sclerosis acts throughout the normal-appearing white matter. Am. J. Neuroradiol. 2006; 27: 868–874.
21. Parry A, Clare S, Jenkinson M, Smith S, Palace J, Matthews PM. White matter and lesion T1 relaxation times increase in parallel and correlate with disability in multiple sclerosis. J. Neurol. 2002; 249: 1279–1286.
22. Castriota-Scanderbeg A, Fasano F, Filippi M, Caltagirone C. T1 relaxation maps allow differentiation between pathologic tissue subsets in relapsing–remitting and secondary progressive multiple sclerosis. Mult. Scler. 2004; 10: 556–561.
23. Filippi M, Rocca MA, Martino G, Horsfield MA, Comi G. Magnetization transfer changes in the normal appearing white matter precede the appearance of enhancing lesions in patients with multiple sclerosis. Ann. Neurol. 1998; 43: 809–814.
24. Pike GB, De Stefano N, Narayanan S, Worsley KJ, Pelletier D, Francis GS, Antel JP, Arnold DL. Multiple sclerosis: magnetization transfer MR imaging of white matter before lesion appearance on T2-weighted images. Radiology 2000; 215: 824–830.
25. Iannucci G, Tortorella C, Rovaris M, Sormani MP, Comi G, Filippi M. Prognostic value of MR and magnetization transfer imaging findings in patients with clinically isolated syndromes suggestive of multiple sclerosis at presentation. Am. J. Neuroradiol. 2000; 21: 1034–1038.
26. Loevner LA, Grossman RI, Cohen JA, Lexa FJ, Kessler D, Kolson DL. Microscopic disease in normal-appearing white matter on conventional MR images in patients with multiple sclerosis: assessment with magnetization-transfer measurements. Radiology 1995; 196: 511–515.
27. Richert ND, Ostuni JL, Bash CN, Duyn JH, McFarland HF, Frank JA. Serial whole-brain magnetization transfer imaging in patients with relapsing–remitting multiple sclerosis at baseline and during treatment with interferon beta-1b. Am. J. Neuroradiol. 1998; 19: 1705–1713.
28. Werring DJ, Clark CA, Barker GJ, Thompson AJ, Miller DH. Diffusion tensor imaging of lesions and normal-appearing white matter in multiple sclerosis. Neurology 1999; 52: 1626–1632.
29. Griffin CM, Dehmeshki J, Chard DT, Parker GJM, Barker GJ, Thompson AJ, Miller DH. T1 histograms of normal-appearing brain tissue are abnormal in early relapsing–remitting multiple sclerosis. Mult. Scler. 2002; 8: 211–216.
30. Allen IV, McKeown SR. A histological, histochemical and biochemical study of the macroscopically normal white matter in multiple sclerosis. J. Neurol. Sci. 1979; 41: 81–91.
31. Barnes D, Munro PM, Youl BD, Prineas JW, McDonald WI. The longstanding MS lesion. A quantitative MRI and electron microscopic study. Brain 1991; 114(3): 1271–1280.
32. Barnes D, McDonald WI, Landon DN, Johnson G. The characterization of experimental gliosis by quantitative nuclear magnetic resonance imaging. Brain 1988; 111(1): 83–94.
33. Evangelou N, Konz D, Esiri MM, Smith S, Palace J, Matthews PM. Regional axonal loss in the corpus callosum correlates with cerebral white matter lesion volume and distribution in multiple sclerosis. Brain 2000; 123(9): 1845–1849.
34. Parry A, Clare S, Jenkinson M, Smith S, Palace J, Matthews PM. MRI brain T1 relaxation time changes in MS patients increase over time in both the white matter and the cortex. J. Neuroimaging 2003; 13: 234–9.
35. Janardhan V, Suri S, Bakshi R. Multiple sclerosis: hyperintense lesions in the brain on nonenhanced T1-weighted MR images evidenced as areas of T1 shortening. Radiology 2007; 244: 823–831.
36. Davies GR, Hadjiprocopis A, Altmann DR, Chard DT, Griffin CM, Rashid W, Parker GJ, Tofts PS, Kapoor R, Thompson AJ, Miller DH.

Normal-appearing grey and white matter T1 abnormality in early relapsing–remitting multiple sclerosis: a longitudinal study. Mult. Scler. 2007; 13: 169–177.
37. Niepel G, Tench CR, Morgan PS, Evangelou N, Auer DP, Constantinescu CS. Deep gray matter and fatigue in MS. J. Neurol. 2006; 253: 896–902.
38. Zellini F, Niepel G, Tench CR, Constantinescu CS. Hypothalamic involvement assessed by T1 relaxation time in patients with relapsing–remitting multiple sclerosis. Mult. Scler. 2009; 15: 1442–1449.
39. Dousset V, Grossman RI, Ramer KN, Schnall MD, Young LH, Gonzalez-Scarano F, Lavi E, Cohen JA. Experimental allergic encephalomyelitis and multiple sclerosis: lesion characterization with magnetization transfer imaging. Radiology 1992; 182: 483–491.
40. Fooladi M, Riyahi AN, Harirchyan MH, Firuznia K, Oghabian MA, Shakiba M, Rafie B, Bakhtiary M. Prognostic value of brain tissue pathological changes in patients with clinically isolated syndromes (CIS) suggestive of multiple sclerosis using magnetization transfer ratio (MTR). Conf. Proc. IEEE Eng. Med. Biol. Soc. 2007; 2007: 2031–2033.
41. Rocca MA, Agosta F, Sormani MP, Fernando K, Tintore M, Korteweg T, Tortorella P, Miller DH, Thompson A, Rovira A, Montalban X, Polman C, Barkhof F, Filippi M. A three-year, multi-parametric MRI study in patients at presentation with CIS. J. Neurol. 2008; 255: 683–691.
42. Fernando KTM, Tozer DJ, Miszkiel KA, Gordon RM, Swanton JK, Dalton CM, Barker GJ, Plant GT, Thompson AJ, Miller DH. Magnetization transfer histograms in clinically isolated syndromes suggestive of multiple sclerosis. Brain 2005; 128: 2911–2925.
43. Brex PA, Leary SM, Plant GT, Thompson AJ, Miller DH. Magnetization transfer imaging in patients with clinically isolated syndromes suggestive of multiple sclerosis. Am. J. Neuroradiol. 2001; 22: 947–951.
44. Gallo A, Rovaris M, Benedetti B, Sormani MP, Riva R, Ghezzi A, Martinelli V, Falini A, Comi G, Filippi M. A brain magnetization transfer MRI study with a clinical follow up of about four years in patients with clinically isolated syndromes suggestive of multiple sclerosis. J. Neurol. 2007; 254: 78–83.
45. Fernando KTM, McLean MA, Chard DT, MacManus DG, Dalton CM, Miszkiel KA, Gordon RM, Plant GT, Thompson AJ, Miller DH. Elevated white matter myo-inositol in clinically isolated syndromes suggestive of multiple sclerosis. Brain 2004; 127: 1361–1369.
46. Wattjes MP, Harzheim M, Lutterbey GG, Bogdanow M, Schild HH, Traeber F. High field MR imaging and ^{1}H-MR spectroscopy in clinically isolated syndromes suggestive of multiple sclerosis. J. Neurol. 2008; 255: 56–63.
47. Wattjes MP, Harzheim M, Lutterbey GG, Klotz L, Schild HH, Traber F. Axonal damage but no increased glial cell activity in the normal-appearing white matter of patients with clinically isolated syndromes suggestive of multiple sclerosis using high-field magnetic resonance spectroscopy. Am. J. Neuroradiol. 2007; 28: 1517–1522.
48. Tillema JM, Leach J, Pirko I. Non-lesional white matter changes in pediatric multiple sclerosis and monophasic demyelinating disorders. Mult. Scler. J. 2012; 18: 1754–1759.
49. Liu Y, Yu C, Li K, Lin F, Duan Y, Qin W. A comparative study of MR diffusion tensor imaging histogram between clinically isolated syndrome and relapsing–remitting multiple sclerosis in normal appearing white matter and grey matter. Chin. J. Radiol. 2008; 42: 341–345.
50. Yu CS, Lin FC, Liu Y, Duan Y, Lei H, Li KC. Histogram analysis of diffusion measures in clinically isolated syndromes and relapsing–remitting multiple sclerosis. Eur. J. Radiol. 2008; 68: 328–334.
51. Caramia F, Pantano P, Di Legge S, Piattella MC, Lenzi D, Paolillo A, Nucciarelli W, Lenzi GL, Bozzao L, Pozzilli C. A longitudinal study of MR diffusion changes in normal appearing white matter of patients with early multiple sclerosis. Magn. Reson. Imaging 2002; 20: 383–388.
52. Vishwas MS, Healy BC, Pienaar R, Gorman MP, Grant PE, Chitnis T. Diffusion tensor analysis of pediatric multiple sclerosis and clinically isolated syndromes. Am. J. Neuroradiol. 2013; 34: 417–423.
53. Reitz LY, Inglese M, Fiehler J, Finsterbusch J, Holst B, Heesen C, Martin R, Schippling S. Quantitative T2′ imaging in patients with clinically isolated syndrome. Acta Neurol. Scand. 2012; 126: 357–363.
54. Varga AW, Johnson G, Babb JS, Herbert J, Grossman RI, Inglese M. White matter hemodynamic abnormalities precede sub-cortical gray matter changes in multiple sclerosis. J. Neurol. Sci. 2009; 282: 28–33.